

π - μ Separation with a 235 gm cm^{-2} Filter*

J. T. Dakin and G. J. Feldman

The Stanford Linear Accelerator Center
Stanford, California 94305

Abstract

The system for distinguishing π 's from μ 's in the SPEAR magnetic detector is described. The probabilities for misidentifying a π as a μ and a μ as a π are determined experimentally.

(Submitted to Nuclear Instruments and Methods)

*Work supported by the U. S. Atomic Energy Commission

A large solid angle magnetic detector has been built at the Stanford Linear Accelerator Center to study the hadronic final states in high energy $e^+ - e^-$ collisions.¹ These collisions occur in the 2.6 GeV storage ring SPEAR. One important feature of the magnetic detector is its ability to distinguish π 's from μ 's. The purpose of this article is to describe the separation method, and a test performed to calibrate the method.

A typical problem for the magnetic detector will be the separation at 2.6 GeV X 2.6 GeV of $e^+e^- \rightarrow \mu^+\mu^-$ from $e^+e^- \rightarrow \pi^+\pi^-$. The rate of the former is predicted in quantum electrodynamics, so its measurement will provide a convenient normalization for other e^+e^- reactions. The rate of the latter determines the π form factor, and is expected to be 3 orders of magnitude smaller than the former. To measure the π form factor we therefore must have a π - μ separation 1) which has a $\ll 10^{-3}$ probability of mis-identifying $\mu^+\mu^-$ as $\pi^+\pi^-$ and 2) whose $\pi^+\pi^-$ losses are known. This level of π - μ separation might easily be provided by a μ range telescope thick enough to bring the 2.6 GeV μ to rest ($\sim 1500 \text{ gm/cm}^2$ of Fe). However, for economic and structural reasons the magnetic detector has been built with a relatively thin, 235 gm/cm^2 "hadron filter" preceded and followed by spark chambers. It is important to verify that this filter is adequate.

The magnetic detector is shaped as a right-cylinder, whose axis (z) is the beam line. A partial cross section of the detector, cut perpendicular to the axis, is shown in Fig. 1. Upon leaving the axis in the plane of Fig. 1 a non-interacting high energy particle passes in succession through the following: a set of spark chambers in a 4-kg magnetic

field, an aluminum wall, a scintillator, an Al solenoid coil, a shower counter, iron flux return, and the muon chambers. The central radii (r) and thicknesses of these objects are shown in Table I. A charged particle passing from the inner spark chambers to the muon chambers undergoes coulomb multiple scattering in the intervening material. The consequent deviations in position and angle from an unscattered trajectory at the muon chambers can be approximated as those due to a 18.4 radiation length scatterer at $r = 1.93$ m. The particle is deflected by the magnetic field in the flux return, which points in the z direction, and has an integrated value $\int B_z dr = 2.61$ kg-m.

We distinguish π 's from μ 's by seeing where a trajectory of known momentum from the inner spark chambers should hit the muon spark chambers, and looking there for sparks. For each spark we compute s , its separation from the (unscattered) trajectory, and σ_s , the rms deviation in s expected from a simple treatment² of the coulomb multiple scattering in the hadron filter. Both s and σ_s are computed projected on the plane of Fig. 1 because the muon spark chambers give no information about the z coordinate of a spark. At this point one of two techniques can be applied for π - μ separation. With the "position" technique we look in both chambers to find the one spark with the smallest absolute value of s/σ_s . If $|s/\sigma_s|$ is less than an arbitrary limit, L , the particle is called a μ . If $|s/\sigma_s| > L$, or no spark is found, the particle is called a π . With the "angle" technique, we find the spark with smallest $|s/\sigma_s|$ in each chamber, and compute θ , the angle between a line through the sparks, and the un-scattered trajectory. Simple theory² is again used to compute σ_θ , the rms deviation expected in θ . If $|\theta/\sigma_\theta| < L$ the particle is called a μ . If $|\theta/\sigma_\theta| > L$,

or either of the chambers has no spark with $|s/\sigma_s| < 4$, the particle is called a π .

With either technique, and a given cut, L , there is some probability that a real π is misidentified as a μ , $P_{\pi\mu}^L$, or that a real μ is misidentified as a π , $P_{\mu\pi}^L$. Each technique has its advantages. The "position" technique uses the chamber information redundantly, reducing the contribution to $P_{\mu\pi}$ due to chamber inefficiency. The "angle" technique minimizes $P_{\pi\mu}$ by making a good geometry π transmission test. Here we report direct measurements of $P_{\pi\mu}^L$ and $P_{\mu\pi}^L$ for both methods, and for various values of L .

These parameters were determined by placing a simulated 0.30 m x 0.30 m segment of the detector wall in a momentum-selected beam containing $\sim 80\%$ π 's, $\sim 19\%$ μ 's and $\sim 1\%$ e 's. The arrangement is shown in Fig. 1.

The spacings and thicknesses of the materials and spark chambers in the test faithfully reproduced those in the detector, as tabulated in Table 1.

The ion flux return in the test, however, was not magnetized. The test apparatus contained additional components providing π - μ identification independent to and more reliable than the detector. These components

were a threshold Cerenkov counter 10 m upstream in the beam, and downstream a 520 gm/cm^2 Fe absorber followed by scintillator C and spark chamber 6.

The Cerenkov counter was set at each beam momentum to detect μ 's with $> 90\%$ efficiency, but to be below threshold pressure for π 's. From

poor-geometry π transmission measurements³ it was estimated that $\approx 2\%$ of the π 's penetrated the full absorber to chamber 6 and to counter C. The

apparatus had 6 gaps of optical spark chamber photographed in a single view — 3 gaps simulating the track chamber, 2 gaps simulating the muon chambers, and the 6th gap after the full absorber. The 2 muon chamber gaps were observed to be $99 \pm 1\%$ efficient each.

Pictures were taken with negative particle beams at 3 momenta -- 1.5, 2.0 and 2.5 GeV/c. The basic beam trigger was a coincidence between 3 beam-defining counters -- one in the Cerenkov counter aperture, and counters A and B in Fig. 1. In addition for " π " pictures, we required that neither the Cerenkov counter nor counter C fire. For " μ " pictures we required that the Cerenkov counter fire. We took ~ 5000 π pictures and ~ 500 μ pictures at each momentum. The beam flux was typically 1 particle per 1.5 μ sec beam pulse.

Pictures containing 1 straight incident track and no other sparks in chambers 1-3 were measured. Sparks were sought in the muon chambers (5 and 6) as described above. In each event we found the best s/σ_s for the position test, and θ/σ_θ for the angle test. Histograms of these quantities for the 2.5 GeV/c μ and π triggers are shown in Fig. 2. A good feeling for the effectiveness of the hadron filter can be achieved by simply comparing the fractions of events in the 2- σ range in the histograms.

We determined $P_{\pi\mu}^L$ from the π -trigger data by counting the fraction of events having $|s/\sigma_s| < L$ or $|\theta/\sigma_\theta| < L$ at each momentum. These fractions were corrected for effects of the π 's which were vetoed by counter C, and of μ 's in the π trigger. The latter were primarily due to π 's which decayed after the Cerenkov counter, and whose decay-product μ 's were not vetoed by counter C. The final values of $P_{\pi\mu}^L$ are presented in Tables II and III. The errors quoted are dominated by the uncertainty in the μ -contamination correction.

It is interesting to compare these measurements of $P_{\pi\mu}$ to more traditional "poor geometry" and "good geometry" π transmissions. From

Blumenthal³ we estimate the poor geometry π transmissions through 235 gm/cm² of Fe at 2.5 GeV/c to be 0.36. This is consistent with our position-separation measurement with a 4 standard deviation cut — $s_{P_{\pi\mu}}^4 = 0.35 \pm 0.02$. From Longo and Moyer⁴ we estimate the corresponding good geometry π transmission to be 0.18. This is consistent with our angle-separation measurement with a 2 standard deviation cut — $\theta_{P_{\pi\mu}}^2 = 0.15 \pm 0.02$.

The μ -losses, $P_{\mu\pi}^L$, were determined from the μ -trigger data. Because they were small, they were subject to large statistical uncertainties, and were sensitive to chamber inefficiency and to π and e contaminations in the μ trigger. To minimize the effects of efficiency and π and e contamination we considered only events for the position test which had $|s/\sigma_s| < 10$, and only events for the angle test which had $|\theta/\sigma_\theta| < 10$. This required us to throw away $\sim 5\%$ of the μ triggers for the former, and $\sim 10\%$ of the μ triggers for the latter. We then determined $P_{\mu\pi}^L$ by counting the fraction of events with $|s/\sigma_s| > L$ or $|\theta/\sigma_\theta| > L$. The values of $P_{\mu\pi}^L$ thus obtained are presented in Tables II and III. The errors quoted are statistical only. Also, presented in Tables II and III and in Fig. 3 are estimates of $P_{\mu\pi}^L$ based on an exhaustive theoretical treatment⁵ of coulomb scattering.

While the values of $P_{\mu\pi}^L$ from the position test (Table II) are in agreement with the theory, the values of $P_{\mu\pi}^L$ from the angle test (Table III) are high by ~ 0.05 . To trace this discrepancy, events of the suspicious class $|s/\sigma_s| < 2$ but $|\theta/\sigma_\theta| > 4$ were studied further. Most of these events contained extra sparks near the μ sparks in the muon chambers, and sometimes a μ spark was judged to be missing. The frequency of these extra sparks, which sometimes rob the μ sparks, is consistent with the expected occurrence of δ -ray production in the hadron filter.⁶ The confusion generated

by these extra sparks sometimes resulted in a Θ measurement which was large, and not the Θ of the muon. This phenomenon is chamber sensitive and may not occur in the magnetic detector muon chambers.

While $P_{\mu\pi}^L$ from the angle method might be reduced to the theoretical limit by a different computer algorithm, we feel that the position method is a more reliable way of achieving low $P_{\mu\pi}$ because it is much less sensitive to single chamber inefficiency.

In summary, we have calibrated the ability of the SPEAR magnetic detector to distinguish π 's from μ 's. This separation is sufficient to separate $\pi^+ \pi^-$ from $\mu^+ \mu^-$ at E beam = 2.6 GeV, the problem discussed earlier. If the position method is used, and the π - μ cut is at 4 standard deviations, then the single μ rejection ($P_{\mu\pi}^4$) is less than 10^{-2} , and the 2- μ rejection is less than 10^{-4} . If the $\pi^+ \pi^-$ event is required to have both π 's satisfy the π requirement, then the $\pi^+ \pi^-$ acceptance is $(1 - P_{\mu\pi}^4)^2 = 0.42 \pm 0.03$. At lower SPEAR energies, where $\pi^+ \pi^-$ is expected to be larger relative to $\mu^+ \mu^-$, less severe cuts can be made, and the $\pi^+ \pi^-$ acceptance will be accordingly larger.

We wish to thank Roger Gearhart for assistance with the beam, and Fred Martin and Rudy Larsen for help in data taking.

REFERENCES

1. R.F. Schwitters, SIAC Report No. SIAC-PUB-1122 (1972) (unpublished).
2. B. Rossi, High Energy Particles (Prentice Hall, New Jersey, 1952), p.p. 62-77. We use $\sigma_{\theta} = (15 \text{ MeV}/\beta c) \sqrt{t}$ where βc and p are the velocity and momentum of the particle, and t the absorber thickness in radiation lengths. To get σ_s we multiply σ_{θ} by the distance from the effective filter position to the muon chamber. These quantities are corrected for effects of non-normal incidence.
3. R.B. Blumenthal, Ph.D. thesis, Harvard University, 1965 (unpublished).
4. M.J. Longo and B.J. Moyer, Phys. Rev. 125, 701 (1962).
5. W.T. Scott, Rev. Mod. Phys. 35, 231 (1963).
6. B. Rossi, op. cit., p.p. 14-17.

TABLE I

object (material)		r (m)	thickness	
			gm/cm ²	L _{rad}
can	(aluminum)	1.49	3.43	.143
scintillator	(plastic)	1.51	2.67	.061
coil	(aluminum)	1.64	24.00	1.000
shower counter	(aluminum)	1.82	6.86	.286
	(plastic)		3.22	.074
	(lead)		34.8	5.34
flux return	(iron)	2.08	<u>160.0</u>	<u>11.5</u>
hadron filter	sub total	1.93 ⁺	235.0	18.4
muon chambers	4	2.31		
	5	2.43		
absorber	(iron)	2.74	<u>520.0</u>	<u>37.3</u>
	total		755.0	55.7

⁺ this is the effective position of the total 18.4 L_{rad} scatterer

Table II

π - μ Separation by Position
at the Muon Chambers

momentum (GeV/c)	s/σ_s cut					
	L = 2		L = 3		L = 4	
	$P_{\pi\mu}^2$	$P_{\mu\pi}^2$	$P_{\pi\mu}^3$	$P_{\mu\pi}^3$	$P_{\pi\mu}^4$	$P_{\mu\pi}^4$
1.5	.28 \pm .03	.060 \pm .020	.34 \pm .03	.020 \pm .012	.38 \pm .03	.007 \pm .007
2.0	.29 \pm .02	.023 \pm .009	.36 \pm .02	.016 \pm .007	.39 \pm .02	.006 \pm .005
2.5	.27 \pm .02	.049 \pm .007	.32 \pm .02	.017 \pm .004	.35 \pm .02	.006 \pm .002
theory		.068		.014		.005

Table III

π - μ Separation by Angle
at the Muon Chambers

momentum (GeV/c)	θ/σ_θ cut					
	L = 2		L = 3		L = 4	
	$P_{\pi\mu}^2$	$P_{\mu\pi}^2$	$P_{\pi\mu}^3$	$P_{\mu\pi}^3$	$P_{\pi\mu}^4$	$P_{\mu\pi}^4$
1.5	.14 \pm .03	.103 \pm .028	.18 \pm .03	.044 \pm .018	.20 \pm .03	.007 \pm .007
2.0	.16 \pm .02	.124 \pm .021	.19 \pm .02	.060 \pm .015	.20 \pm .02	.039 \pm .012
2.5	.15 \pm .02	.124 \pm .011	.18 \pm .02	.065 \pm .008	.20 \pm .02	.049 \pm .007
theory		.068		.014		.005

FIGURE CAPTIONS

1. The apparatus. A schematic cross section of the SPEAR magnetic detector, cut perpendicular to the beam axis, is shown. The simulated segment of the detector wall used in the test is drawn on top and shaded. The 6 spark chambers used in the test are labeled 1-6, and the 3 scintillation counters are labeled A, B and C.
2. The 2.5 GeV/c raw muon chamber data. Histograms are shown of the deviation of the closest spark (s/σ_s) for (a) the μ trigger and (b) the π trigger, and of the deviation of the angle (θ/σ_θ) for (c) the μ trigger and (d) the π trigger. In each histogram the fraction of the triggers having $|s/\sigma_s| < 2$ or $|\theta/\sigma_\theta| < 2$ is indicated.
3. The theoretical function $P_{\mu\pi}^L$ for this hadron filter based on the treatment of multiple coulomb scattering in Ref. 5 (solid line). For comparison the simple Gaussian assumption is also shown (dashed line).

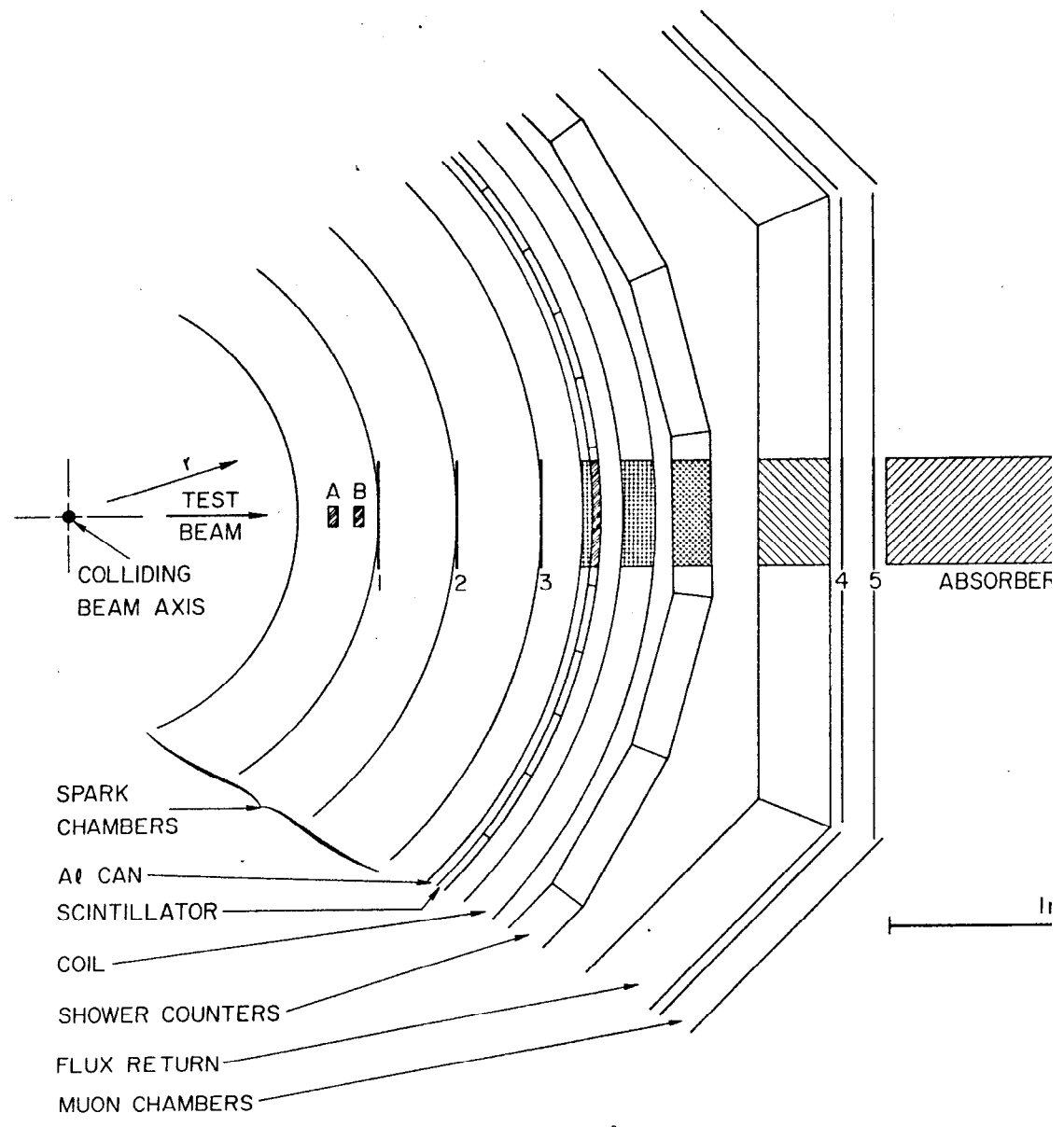
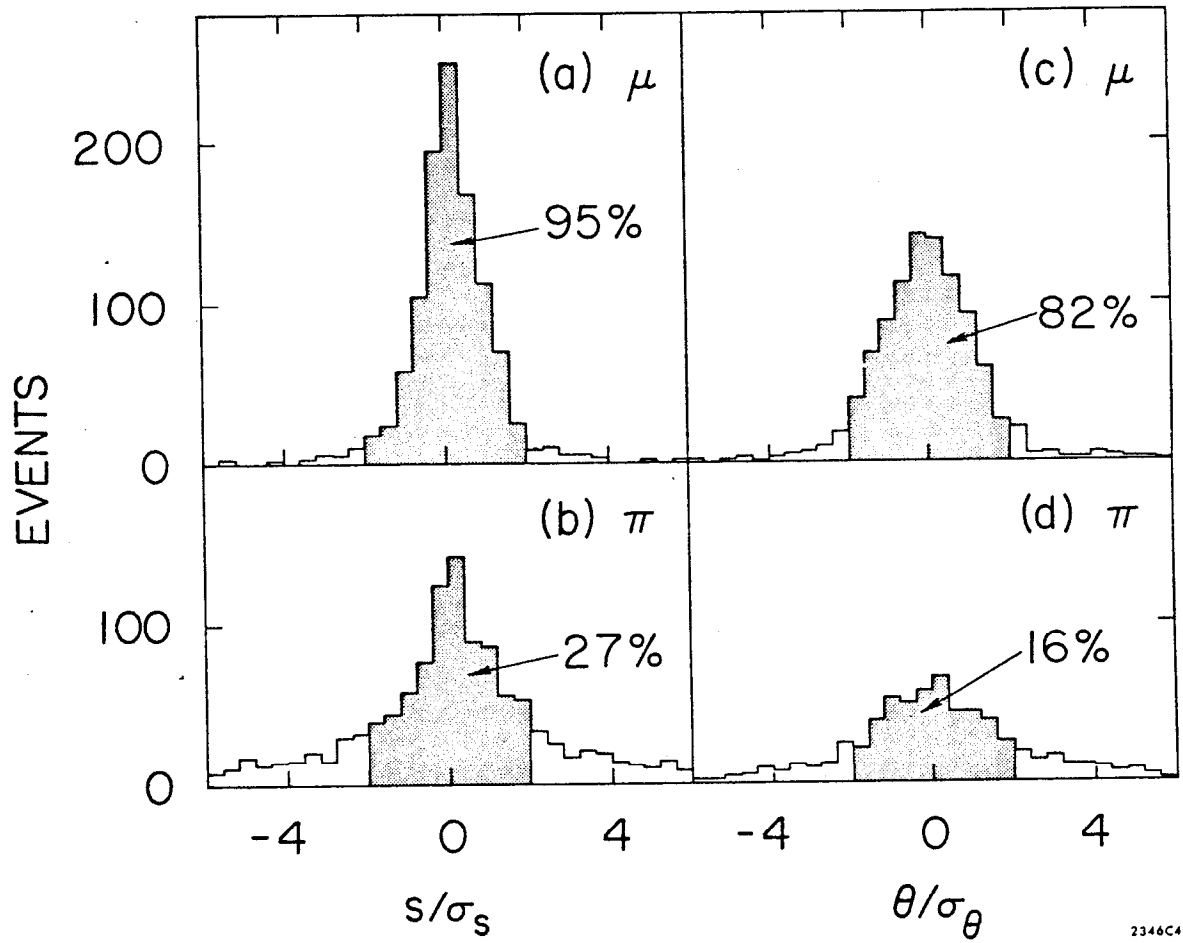


Fig. 1



2346C4

Fig. 2

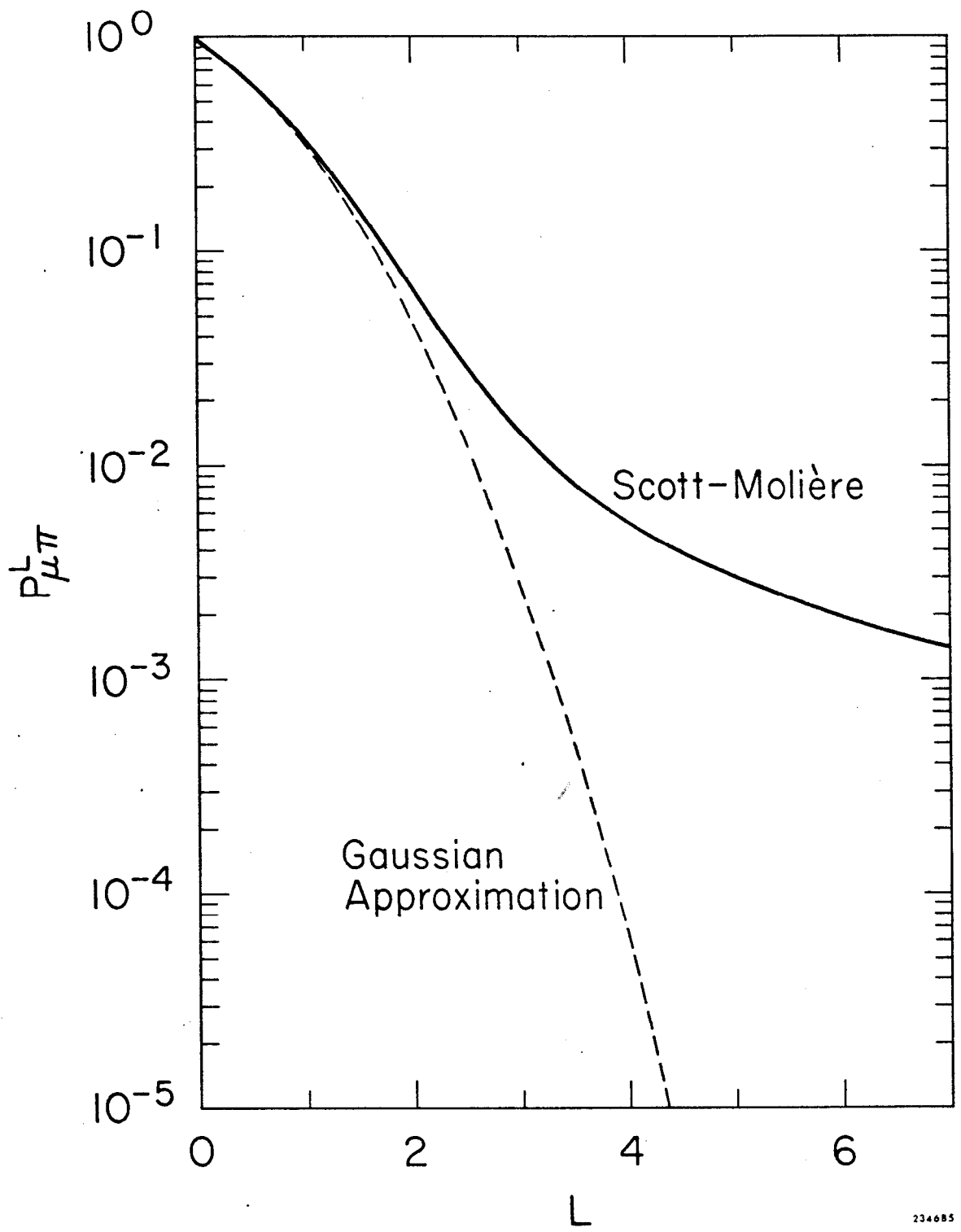


Fig. 3